# The bond-behaviour of CFRP-to-concrete bonded joints under fatigue loading: A damage accumulation model

# The bond-behaviour of CFRP-to-concrete bonded joints under fatigue loading: a damage accumulation model

Hao Zhou[1], Shishun Zhang[2], Dilum Fernando[3,*], Tianli Huang[1]

[1]School of Civil Engineering, Central South University, Changsha 410075, China

[2]School of Civil and Hydraulic Engineering, Huazhong University of Science and Technology, Wuhan 430074, China

[3]School of Engineering, University of Edinburgh, Edinburgh, EH9 3FB, Scotland, UK

Corresponding author: dilum.fernando@ed.ac.uk

**Abstract:**

This paper presents a theoretical study aimed at predicting the behaviour of carbon fibre reinforced polymer-to-concrete bonded joints under fatigue-cyclic loading. A model considering the plastic deformations of the interface, the damage, and the damage accumulation due to fatigue-cyclic loading is proposed. The damage accumulation model is calibrated through the experimental bond-slip relation. Then, a numerical algorithm is formulated to simulate the fatigue bond behaviour using the calibrated damage accumulation model. Numerical simulation was found to provide conservative predictions for fatigue life, which was attributed to the neglect of beneficial effects from the compression stress state near the loaded end in the single-shear pull-off test.

**Keywords:** CFRP strengthening; bond behaviour, fatigue loading, damage accumulation model

## 1 Introduction

Carbon fibre reinforced polymer (CFRP) strengthening of reinforced concrete (RC) structures to increase flexural and shear capacities has become a popular technique amongst the construction engineers due to its many advantages such as high strength-to-weight ratio, ease of application, and less disturbance to traffic [1, 2]. Amongst the numerous strengthening techniques using CFRPs, the externally bonded (EB) CFRP laminate strengthening technique that requires minimal efforts to implement has been the most popular technique. Performance of RC structures strengthened using EB CFRP relies on the interfacial shear stress transfer mechanism of the CFRP-to-concrete (FC) bonded joints [3]. Therefore, understanding the behaviour of FC bonded joints is of key significance. As a result, many efforts have been devoted to understanding and predicting the bond behaviour of FC bonded joints [4-8]. Design theories have been well established to predict the behaviour of FC bonded joints under quasi-static monotonic loading [4, 5]. In these prediction models, a bond-slip relation which describes the relation between the interfacial shear stress and the relative displacement between the CFRP and concrete substrate, is commonly used for modelling the behaviour of FC bonded joints under monotonic loading [5,9]. In such bond-slip models, a damaged elasticity assumption (i.e., load is assumed to always unload to zero at zero slip) is often made for defining damage evolution.

Many EB CFRP strengthened RC structures, such as bridge girders are likely to be subjected to repeated loading. Such repeated loading can be generally categorized into quasi-static cyclic loading and fatigue-cyclic loading according to the loading frequency. For simplicity, the former will be termed as cyclic loading and the latter as fatigue loading in this paper. Compared to the research on the bond behaviour under monotonic loading, only limited research has been carried out so far on understanding the behaviour of FC bonded joints under cyclic loading [9-14]. Existing experimental investigations have shown that when subjected to cyclic loading, FC bonded joints also fail within concrete (i.e. cohesion failure within concrete) similarly to those joints subjected to monotonic loading [14].

Experimentally derived bond-slip relations under cyclic loading showed clear damage plasticity (i.e. reduction in unloading stiffness due to damage and residual slip at zero load during unloading showing plastic deformations) behaviour [11, 14, 15] therefore shows the commonly used damage elasticity assumption in representing the cyclic bond behaviour is not accurate [3, 16]. Several analytical models have been proposed to predict the cyclic bond behaviour of the FC bonded joints considering damaged plasticity [12-14]. Different from bond-slip relations under monotonic loading, bond-slip relations under cyclic loading require damage parameters to be defined considering both damage and plasticity during unloading/reloading within the softening range. Zhou et al. [14] pointed out several shortcomings of the existing models and proposed the first thermodynamically consistent bond-slip relation for FC bonded joints under cyclic loading. However, existing experimental studies on FC bonded joints under fatigue loading have shown that failure modes are more complex than that of FC bonded joints under monotonic or cyclic loading [17-25], thus bond-slip models derived for monotonic or cyclic loading cannot be directly applied to FC bonded joints under fatigue loading.

Different failure modes including cohesion failure within the concrete, cohesion failure within the adhesive, adhesion failure at the CFRP-adhesive bi-material interface, adhesion failure at the concrete-adhesive bi-material interface, and interlaminar failure within the CFRP laminate were observed in FC bonded joint tests under fatigue loading [18, 20-23, 26]. Amongst the failure modes observed, adhesion failures are subjected to the quality of surface preperation. However, studies reporting the adhesion failures often did not report surface quality measurements or sufficient details of the adopted surface preparation methods. Therefore, it is difficult to asses if the adhesion failure was driven by the poor surface quality. On the otherhand, existing research has shown that with adequate surface preperation, adhesion failure modes of the FC bonded joints (i.e. adhesion failure at the CFRP-adhesive and the concrete-adhesive bi-material interfaces) can be avoided [26]. Once adhesion failures are avoided, failure mode under fatigue loading was found to be dependent on the concrete strength, the CFRP laminate type and the maximum fatigue load level [27]. To date the exact reasons for complex failure modes observed under fatigue loading remain largely unknown. More

studies are required to better understand the change of failure modes in FC bonded joints under fatigue loading. Nonetheless, while the effect of CFRP laminate type on the overall fatigue performance is not clear, the selection of a certain type of CFRP laminate (e.g. MasterBrace Laminate) was found to to avoid the CFRP interlaminar failure and the failures were limited to cohesion failure within concrete or cohesion failure within adhesive [27]. Experimental studies of FC bonded joints under fatigue loading showed a decrease in the slope of the load-displacement curve with the increasing number of loading cycles [19-26]. Softening of the interface and the gradual debonding of the CFRP laminate from the concrete substrate are believed to be the reasons for the observed degradation of stiffness of the load-displacement curves.

It is common to assess the performance of a bonded joint in terms of its fatigue life (i.e. number of loading cycles the bonded joint can sustain), thus has been the key focus of the majority of the published work on FC bonded joints under fatigue loading [18, 21, 25, 28, 29]. To the best of the author's knowledge, only two studies have been published so far on the experimental bond-slip behaviour of FC bonded joints under fatigue loading [23, 26]. Both studies showed an obvious damage accumulation in unloading/reloading stiffness of the bond-slip relation because of the fatigue loading. Existing experimental investigations on FC bonded joints under fatigue loading [27] have demonstrated that if elastic interfacial shear stresses are less than 80% of the maximum interfacial shear strength, fatigue loading would not cause any damage. When loaded beyond this stress level, damage due to fatigue will initiate and starts to accumulate. A similar conclusion can be found in Al-Saoudi et al. [30] in which the fatigue damage threshold value of the stress was found to be 75% of the maximum interfacial shear strength under monotonic loading.

Several theoretical models have been proposed to predict the fatigue life of FC bonded joints [22, 25, 26, 31, 32], the rate of debonding [18, 28], and the bond-slip relation under fatigue loading [13, 23, 33]. Among which, Zhu et al. [26] and Li et al. [22] expressed the fatigue life of FC bonded joints as a function of the loading amplitude and the concrete compressive strength. However, the fatigue life of the bonded joints is also affected by the interface geometry (e.g., CFRP laminate thickness,

adhesive thickness) which affects the interfacial stress significantly. Therefore, both models cannot be applied for bonded joints of different geometries. Carrara and De Lorenzis [13] proposed a damage-plasticity model to capture the behaviour of the bonded interface under fatigue loading. Their model assumed unloading of the slip with zero interfacial shear stress. However, this assumption was later proven to be unreasonable by experimental results of FC bonded joints under cyclic loading [14]. Recent study by Zhang et al. [33] presented a mix-mode cohesive zone model to simulate the bond behaviour of FC bonded joints under fatigue loading. Stiffness degradation of the traction-separation curves was not related to the number of loading cycles. Empirical-based equations were developed for load degradation as a function of the number of loading cycles. Such a model however does not appropriately consider the fatigue damage of the interface as a function of the loading applied to the interface, thus cannot be used in general for modelling fatigue behaviour of any FC bonded interface.

It should be noted that none of the existing models considered the possibility of fracture surface moving from one constituent to another. As the interfacial fracture work is directly related to the constituent where the fracture would occur, a change in the failure mode affects the total fracture work thus the damage process. Therefore, if the fracture path is different, models ignoring the failure mode change cannot be directly applied.

Against this background, this paper presents a theoretical study aimed at developing a bond-slip relation for FC bonded joints under fatigue loading, when the failure mode is cohesion failure within concrete. The present study is built upon the previous experimental work carried out by the authors on FC bonded joints subjected to fatigue loading [27]. Only the “cohesion failure within concrete” failure mode was considered due to lack of data available on FC bonded joints subjected to fatigue loading and failing in other failure modes. In the present study, a finite difference (FD) algorithm was firstly formulated to simulate the bond behaviour of FC bonded joints under fatigue loading. Then, a path-defined model was proposed to simulate the unloading and reloading of bond-slip relation under fatigue loading. Based on the experimental results of FC bonded joints failed within concrete, the damage accumulation rate was calibrated through regression analysis and was implemented in the

proposed FD algorithm. The load-displacement curve and the local bond-slip relation from the numerical predictions were compared with test results.

## 2 The proposed model

### *2.1 Simulation of the CFRP-to-concrete bonded joints under fatigue loading*

The bond behaviour of FC bonded joints is often investigated through a single-shear pull-off test (Fig. 1). By assuming that the interfacial shear stresses are uniform through the thickness of the adhesive layer and ignoring the bending and longitudinal normal stresses in the adhesive layer, the free body diagram of an indefinite segment can be drawn as Fig. 1c. These assumptions, also commonly adopted in other research, were shown to have a negligible effect on the simulation of the behaviour of FC bonded joints under mode II loading [7, 12, 34]. To simulate the bond behaviour of FC bonded joints under fatigue loading, the FD method proposed by Carrara and Ferretti [34] was modified to account for the change in bond-slip relation when fatigue loading is applied. Detailed FD method is presented below.

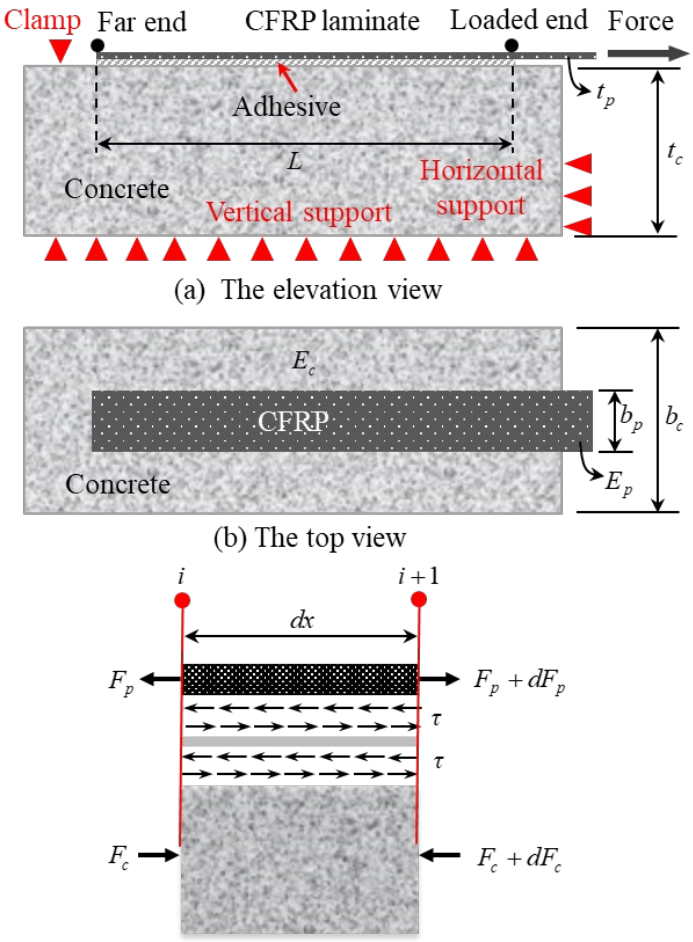


138

139 **Fig.1.** Idealized CFRP-to-concrete (FC) bonded joints

140 According to the force equilibrium of the CFRP element shown in Fig. 1c, the following differential

141 equation can be established:

142 $$\frac{dF_p}{dx} = \tau b_p \tag{1}$$

143 where $F_p$ and $b_p$ are the axial force and width of the CFRP plate respectively, $\tau$ is the interfacial

144 shear stress acting at the bi-material interface with segment length $dx$.

145 The relative displacement between the CFRP plate and the concrete substrate, i.e., slip ($\delta$) can be

146 written as follows:

147 $$\delta = u_p - u_c \tag{2}$$

Where $u_p$ and $u_c$ are the displacements of CFRP plate and concrete at a given position of the bonded joints respectively.

For the CFRP laminate and the concrete under axial loading, the constitutive relation can be written as:

$$\sigma_p = E_p \frac{du_p}{dx} \tag{3}$$

$$\sigma_c = E_c \frac{du_c}{dx} \tag{4}$$

where $E_p$ and $E_c$ are the elastic moduli of the CFRP plate and concrete respectively, and $\sigma_p$ and $\sigma_c$ are the axial stresses of the CFRP plate and the concrete respectively. The axial stresses of the CFRP plate and the concrete can be also written as:

$$\sigma_p = \frac{F_p}{A_p} \tag{5}$$

$$\sigma_c = \frac{F_c}{A_c} \tag{6}$$

where $F_c$ is the axial force applied on the concrete block, $A_p$ and $A_c$ are the sectional areas of CFRP laminate and concrete substrate respectively. According to the force equilibrium at any section, the following equation can be derived:

$$F_p + F_c = 0 \tag{7}$$

From Eqs (2)-(7), the following equation can be derived:

$$\frac{d\delta}{dx} = \left( \frac{1}{E_p A_p} + \frac{1}{E_c A_c} \right) F_p \tag{8}$$

Dividing the whole bonding interface into $n$ number of segments, Eqs (1) and (8) at each segment $i$ (Fig.1c) can be approximated as:

$$\frac{F_p^{i+1} - F_p^i}{h_i} = \frac{1}{2}\left[\tau^{i+1} + \tau^i\right] b_p \tag{9}$$

$$\frac{\delta^{i+1} - \delta^i}{h_i} = \frac{1}{2}\left(\frac{1}{E_p A_p} + \frac{1}{E_c A_c}\right)\left(F_p^{i+1} + F_p^i\right) \tag{10}$$

where $h_i$ is the length of the segment, $\delta^i, \tau^i, F_p^i$ are the slip, interfacial shear stress and axial force of CFRP at node $i$, respectively. When a bilinear bond-slip relation is adopted, the interfacial shear stress can be calculated as:

$$\tau^i = \tau_f^i + K_t^i\left(\delta^i - \delta_1^i\right) \tag{11}$$

where $\tau_f^i$ and $K_t^i$ are the peak shear stress and the tangential stiffness of the bond-slip relation in a given loading cycle. $\delta_1^i$ is the slip value at the peak shear stress at node $i$ in a particular loading cycle. Experimental observations showed that when fatigue loading was stopped and followed by monotonic loading, the bond behaviour has followed the envelope bond-slip relation under monotonic loading [27]. Therefore, it is assumed that for slip values greater than $\delta_1^i$, the slope of the softening curve will be the same as the softening branch of the bond-slip curve under monotonic loading, i.e. $K_s$. Therefore, $K_t^i$ can be calculated as:

$$K_t^i = \begin{cases} \left(1 - D^i\right) K_e & if\ \ \delta_e^i < \delta < \delta_1^i \\ K_s & if\ \ \delta_1^i < \delta < \delta_f^i \\ 0 & if\ \ \delta_f^i < \delta \end{cases} \tag{12}$$

where $K_e$ and $K_s$ are the initial tangential stiffness in the ascending branch and the slope of the softening branch of the bond-slip relation respectively (Fig. 2), $D^i$ is the damage parameter at node

183 *i,* and $\delta_1^i, \delta_e^i$, and $\delta_f^i$ are the slip values at the peak shear stress, zero shear stress and the full damage
184 point at node $i$ respectively. Experimental studies showed that once damage initiates, the value of the
185 $D^i$ increases gradually until the full damage is reached [26]. Therefore, a model to define the
186 variation of $D^i$ (i.e., a damage accumulation model presented in Section 2.2) in Eq. (12) is necessary.

187 During unloading, it is possible that interfacial shear stress becomes negative. In such a case, the
188 tangential stiffness can be found by using the centre-symmetrical point of the slip values with respect
189 to $\delta_e^i$.

190 At the $k^{th}$ step, substituting Eq. (11) into Eq. (9) gives:

191 $$\frac{F_{p,k}^{i+1} - F_{p,k}^{i}}{h_i} = \frac{1}{2}\left[\tau_{f,k}^{i+1} + K_{t,k}^{i+1}\left(\delta_k^{i+1} - \delta_{1,k}^{i+1}\right) + \tau_{f,k}^{i} + K_{t,k}^{i}\left(\delta_k^{i} - \delta_{1,k}^{i}\right)\right] b_p \tag{13}$$

192 As shown in Fig. 2, if the damage parameter is known, the maximum interfacial shear stress ( $\tau_{f,k}$ )
193 and the corresponding slip value ( $\delta_{1,k}$ ) at different nodes in a particular loading cycle can be
194 calculated and will be a constant value within that loading cycle. Therefore, Eq. (10) can be rewritten
195 as:

196 $$\frac{\left(\delta_k^{i+1} - \delta_{1,k}^{i+1}\right) - \left(\delta_k^{i} - \delta_{1,k}^{i}\right)}{h_i} = \frac{1}{2}\left(\frac{1}{E_p A_p} + \frac{1}{E_c A_c}\right)\left(F_{p,k}^{i+1} + F_{p,k}^{i}\right) - \frac{\left(\delta_{1,k}^{i+1} - \delta_{1,k}^{i}\right)}{h_i} \tag{14}$$

197

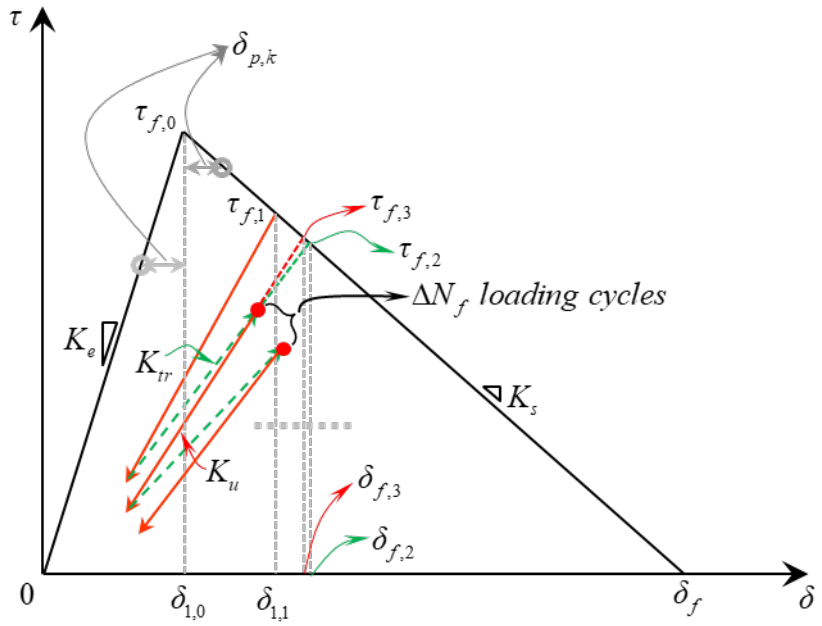


198

199 **Fig.2.** The proposed bond-slip model under fatigue loading.

200 Taking $\delta_{d,k}^{i} = \delta_{k}^{i} - \delta_{1,k}^{i}$ and $\delta_{d,k}^{i+1} = \delta_{k}^{i+1} - \delta_{1,k}^{i+1}$, Eqs (13) and (14) can be expressed respectively as:

201
$$-\frac{F_{p,k}^{i}}{h_i} - \frac{1}{2}K_{t,k}^{i}\delta_{d,k}^{i}b_p + \frac{F_{p,k}^{i+1}}{h_i} - \frac{1}{2}K_{t,k}^{i+1}\delta_{d,k}^{i+1}b_p = \frac{1}{2}\left(\tau_{f,k}^{i+1} + \tau_{f,k}^{i}\right)b_p \tag{15}$$

202
$$-\frac{W}{2}F_{k}^{i} - \frac{\delta_{d,k}^{i}}{h_i} - \frac{W}{2}F_{k}^{i+1} + \frac{\delta_{d,k}^{i+1}}{h_i} = -\frac{\left(\delta_{1,k}^{i+1} - \delta_{1,k}^{i}\right)}{h_i} \tag{16}$$

203 where $W = \dfrac{1}{E_p A_p} + \dfrac{1}{E_c A_c}$. Expressing Eqs (15) and (16) in matrix form gives:

204
$$\begin{bmatrix} -\frac{1}{h_i} & -\frac{1}{2}K_{t,k}^{i}b_p & \frac{1}{h_i} & -\frac{1}{2}K_{t,k}^{i+1}b_p \\ -\frac{1}{2}W & -\frac{1}{h_i} & -\frac{1}{2}W & \frac{1}{h_i} \end{bmatrix} \begin{bmatrix} F_{p,k}^{i} \\ \delta_{d,k}^{i} \\ F_{p,k}^{i+1} \\ \delta_{d,k}^{i+1} \end{bmatrix} = \begin{bmatrix} \frac{1}{2}\left(\tau_{f,k}^{i+1} + \tau_{f,k}^{i}\right)b_p \\ -\frac{\left(\delta_{1,k}^{i+1} - \delta_{1,k}^{i}\right)}{h_i} \end{bmatrix} \tag{17}$$

205 Eq. (17) can be extended to model the full bond joint using the system of equations as:

$$\begin{bmatrix} \mathbf{J}_1 & \mathbf{Q}_1 & & & & & & \\ & \mathbf{J}_2 & \mathbf{Q}_2 & & & & & \\ & & \ddots & \ddots & & & & \\ & & & \mathbf{J}_i & \mathbf{Q}_i & & & \\ & & & & \ddots & \ddots & & \\ & & & & & \mathbf{J}_n & \mathbf{Q}_n & \\ \mathbf{B}_1 & & & & & & & \mathbf{B}_{n+1} \end{bmatrix} \begin{bmatrix} \mathbf{U}_1 \\ \mathbf{U}_2 \\ \vdots \\ \mathbf{U}_i \\ \vdots \\ \mathbf{U}_n \\ \mathbf{U}_{n+1} \end{bmatrix} = \begin{bmatrix} \mathbf{R}_1 \\ \mathbf{R}_2 \\ \vdots \\ \mathbf{R}_i \\ \vdots \\ \mathbf{R}_n \\ \mathbf{Z} \end{bmatrix} \tag{18}$$

The above equation can be also written as $\mathbf{C} \times \mathbf{U} = \mathbf{R}$, where $\mathbf{C}$ is the coefficients matrix composed of $\mathbf{J}_i$ and $\mathbf{Q}_i$ which are given by:

$$\mathbf{J}_i = \begin{bmatrix} -\frac{1}{h_i} & -\frac{1}{2}K_{t,k}^{i} b_p \\ -\frac{1}{2}W & -\frac{1}{h_i} \end{bmatrix}, \ \mathbf{Q}_i = \begin{bmatrix} \frac{1}{h_i} & -\frac{1}{2}K_{t,k}^{i+1} b_p \\ -\frac{1}{2}W & \frac{1}{h_i} \end{bmatrix} \tag{19}$$

$\mathbf{U}_i$ and $\mathbf{R}_i$ in the matrixes $\mathbf{U}$ and $\mathbf{R}$ are given by:

$$\mathbf{U}_i = \begin{bmatrix} F_{p,k}^{i} \\ \delta_{d,k}^{i} \end{bmatrix}, \ \mathbf{R}_i = \begin{bmatrix} \frac{1}{2}\left(\tau_{f,k}^{i+1} + \tau_{f,k}^{i}\right) b_p \\ -\frac{\left(\delta_{1,k}^{i+1} - \delta_{1,k}^{i}\right)}{h_i} \end{bmatrix} \tag{20}$$

$\mathbf{B}_1$ and $\mathbf{B}_{n+1}$ in Eq. (18) are used to implement the boundary conditions, which are dependent on the load type (i.e., force or displacement) and $\mathbf{Z}$ in Eq. (18) is the corresponding force or displacement vector at the loaded end. For fatigue loading of single shear pull-off tests on FC bonded joints presented in Zhou et al. [27], the force control method was used for the initial monotonic loading and the subsequent fatigue loading. However, the displacement control method was used for the final monotonic loading to failure. Therefore, both force and displacement boundary conditions should be considered in simulating the single-shear pull-off tests under fatigue loading presented in Zhou et al. [27]. For the test using force control, the boundary conditions are:

$$\mathbf{B}_1=\begin{bmatrix}1 & 0\\ 0 & 0\end{bmatrix},\quad \mathbf{B}_{n+1}=\begin{bmatrix}0 & 0\\ 1 & 0\end{bmatrix},\quad \mathbf{Z}=\begin{bmatrix}0\\ F^{n+1}\end{bmatrix} \tag{21}$$

Substituting the boundary conditions in Eq. (21) in to Eq. (18) and expanding the expression yields:

$$1\times F_{p,k}^{1}+0\times\delta_{d,k}^{1}+0\times F_{p,k}^{n+1}+0\times\delta_{d,k}^{n+1}=0 \tag{22}$$

$$0\times F_{p,k}^{1}+0\times\delta_{d,k}^{1}+1\times F_{p,k}^{n+1}+0\times\delta_{d,k}^{n+1}=F_{p,k}^{n+1} \tag{23}$$

in which Eq. (22) represents no force is applied at the far end of the CFRP plate, while Eq. (23) means non-zero force is applied at the loaded end.

When the displacement-controlled loading is used, the boundary conditions can be considered as follows:

$$\mathbf{B}_1=\begin{bmatrix}1 & 0\\ 0 & 0\end{bmatrix},\quad \mathbf{B}_{n+1}=\begin{bmatrix}0 & 0\\ 0 & 1\end{bmatrix},\quad \mathbf{Z}=\begin{bmatrix}0\\ \delta_{d,k}^{n+1}\end{bmatrix} \tag{24}$$

Substituting the boundary conditions in Eq. (24) into Eq. (18) and expanding the expression yields:

$$1\times F_{p,k}^{1}+0\times\delta_{d,k}^{1}+0\times F_{p,k}^{n+1}+0\times\delta_{d,k}^{n+1}=0 \tag{25}$$

$$0\times F_{p,k}^{1}+0\times\delta_{d,k}^{1}+0\times F_{p,k}^{n+1}+1\times\delta_{d,k}^{n+1}=\delta_{d,k}^{n+1} \tag{26}$$

which represent a displacement loading boundary condition applied at the loaded end of the CFRP plate.

Once $\delta_{d,k}^{i}$ is solved iteratively, the interfacial shear slip at each node along the bonding length can be calculated from the following expression:

$$\delta_k^i=\delta_{d,k}^i+\delta_{1,k}^i \tag{27}$$

and the interfacial shear stress can be determined from Eq. (11).

238 It can be seen from the above FD algorithm that the $K_t^i$, therefore $D^i$ is critical in simulating the
239 bond behaviour under fatigue cyclic loading. To account for the variation of $K_t^i$ under fatigue loading,
240 $D^i$ should be updated when fatigue cyclic loading is applied. A fatigue damage accumulation model,
241 which describes the variation of $D^i$ with fatigue loading is presented next.

242 ***2.2 The fatigue damage accumulation rate model***

243 Zhou et al. [14] presented a model to determine the damage parameter evolution of FC bonded joints
244 during cyclic loading. In this model, the unloading and reloading were assumed to be the same, such
245 an assumption is also adopted in Roe and Siegmund [35] and Zhang et al. [33]. However, actual
246 loading and unloading behaviour of FC bonded joints demonstrate hysteretic loops [14]. Nonetheless,
247 existing studies on FC bonded joints subjected to cyclic loading have demonstrated that ignoring the
248 hysteretic behaviour in bond-slip models have negligible effects on the overall behaviour of the FC
249 bonded joint [14, 32, 34]. However, assuming the same stiffness in loading and unloading cannot
250 capture the damage accumulation unless the unloading reached the inverse softening region or the
251 loading reached the envelope curve [14].

252 In the present study, in addition to the unloading/reloading curve, a transition path (dashed line in Fig.
253 2) is defined to capture the damage accumulation between two unloading/reloading curves. Different
254 from the reloading path, the transition path represents the damage parameter evolution for every
255 $\Delta N_f$ number of fatigue loading cycles. In this study, the minimum $\Delta N_f$ was taken as 20, as the
256 experimental data in Zhou et al. [27] was recorded at every 20 cycles.

257 While finding the proper function to represent the damage parameter increment, the following
258 characteristics of the bond-slip relation of FC bonded joints subjected to fatigue loading were
259 considered:

260 (1) The damage under fatigue loading was assumed to occur only if the maximum interfacial
261 shear stress is higher than 80% of the peak shear strength under monotonic loading [27]. When

a bi-linear bond-slip relation is employed in the simulation, the same ratio can be used for the slip value at interfacial shear stress when the fatigue damage starts to accumulate.

(2) the damage accumulation rate was assumed to decrease with the damage level. Once the fatigue loading was stopped and monotonic loading was applied, the bond-slip relationship tends to follow the envelope bond-slip curve under monotonic loading.

With the above two considerations, the damage evolution law for both unloading/reloading and transition stiffness is expressed as:

$$\dot{D}_{ur/tr} = \alpha_{ur/tr} \times \left(1 - D_{ur/tr}\right) \times \exp\left(\beta_{ur/tr} \times D_{ur/tr}\right) \times \Delta \tag{28}$$

where $\dot{D}_{ur/tr}$ is the damage accumulation rate for the unloading/reloading stiffness ($D_{ur}$) or transition stiffness ($D_{tr}$) with respect to the loading cycles. It should be noted that the transition stiffness is the slope of the curve representing the path between different loading cycles, thus it only carries a numerical meaning in this study. $\Delta$ is a parameter to account for loading amplitude effect on the damage accumulation rate, and is given as:

$$\Delta = \left[ \left\langle \frac{\delta_{\max}}{\delta_{1,0}} \right\rangle_{+} \times \frac{\delta_{\max} - \delta_{\min}}{\delta_{1,0}} \right] \tag{29}$$

where $\delta_{\max}$ and $\delta_{\min}$ are the maximum and minimum slips the node can reach within the loading cycle, $\delta_{1,0}$ is the slip value corresponding to the maximum shear stress of the initial bond-slip relation under monotonic loading, and $\langle\ \rangle_{+}$ is an operator defined as:

$$\langle \eta \rangle_{+} = \begin{cases} \eta & if \quad \eta \geq r_{cri} \\ 0 & if \quad \eta < r_{cri} \end{cases} \tag{30}$$

where $r_{cri}$ is the critical ratio when the fatigue damage starts to accumulate (in this study, $r_{cri}=0.8$ is considered based on the test results presented in Zhou et al. [27]). $r_{cri}$, $\alpha_{ur/tr}$ and $\beta_{ur/tr}$ are empirical parameters calibrated from the experimentally obtained bond-slip relations under fatigue cyclic loading.

As the damage accumulation rate under fatigue loading depends on both the current damage parameter and the loading amplitude, the damage parameter in the unloading/reloading or transition path under fatigue loading should be updated as follows:

$$D^i_{ur/tr,tot}\Big|_t = D^i_{ur/tr}\Big|_{t-\Delta t} + \Delta t \times \dot{D}^i_{ur/tr}\Big|_{t-\Delta t} \tag{31}$$

where $t$ is the pseudo time, which could be the number of loading cycles, and $\Delta t$ is the number of loading cycles when the damage parameter is updated. $D^i_{ur/tr}\Big|_{t-\Delta t}$ is the damage parameter of unloading/reloading or transition stiffness at the $i^{th}$ node at time $t-\Delta t$.

### *2.3 The bond-slip relation of CFRP-to-concrete bonded joints subjected to fatigue loading*

A complete bond-slip relation of a FC bonded joint under fatigue loading is illustrated in Fig.3. As mentioned previously, the damage parameter during the initial monotonic/cyclic loading of the bonded joint can be calculated with the damage-plasticity model proposed in Zhou et al. [14]. In which the damage parameter as a function of the ratio between the dissipated energy and the total fracture energy. Once fatigue loading is applied, no damage will accumulate until the slip at that point reach the critical value $\delta_{cri}=r_{cri}\delta_{f,0}$ ($S_1$ in Fig.3) in which $r_{cri}=0.8$ is assumed according to previous research by the authors group [27]. Beyond this slip, fatigue damage will start to accumulate. For a point already in the softening stage ($S_2$ in Fig. 3), the damage parameter can be calculated from the unloading/reloading stiffness, as the greater value between the value calculated from Eq. (31) and the one from the damage-plasticity model under cyclic loading (i.e. Zhou et al. [14] model). It is assumed

that the change in damage parameter can only occur at the minimum slip point ($S_3$ in Fig. 3) for the transition stiffness, and the maximum slip point ($S_4$ in Fig. 3) for the unloading/reloading stiffness

So far to the best of the authors' knowledge, no experimental data exists on FC bonded joints under reversed cyclic loading, thus the behaviour of the FC bonded joints under reverse cyclic loading remains largely unknown. In bond-slip relation of FC bonded joints, the total layers between the underside of the CFRP laminate and the final fracture surface in concrete are considered as a single layer. To date the most detailed explanation of fracture propagation process in FC bonded joints was provided by Lu et al. [36]. Lu et al. [36] explained that under interfacial stresses, multiple diagonal cracks may occur within concrete near the adhesive-concrete interface resulting in mesoscale columns. At some stage, due to tensile stresses created by bending of those meso-scale columns, fracture parallel to the axis of the bonded joint will occur. Reversal of the shear forces may create new fracture lines orthogonal to the original diagonal cracks. In addition, reversal of the shear cracks will also reverse the direction of bending of the meso-scale columns. Therefore, it is not possible to provide a simple solution for reversal of bond-slip relation assuming reversal of plasticity. More investigations are necessary to understand the mechanisms occurring at the bonded joints under reverse cyclic loading.

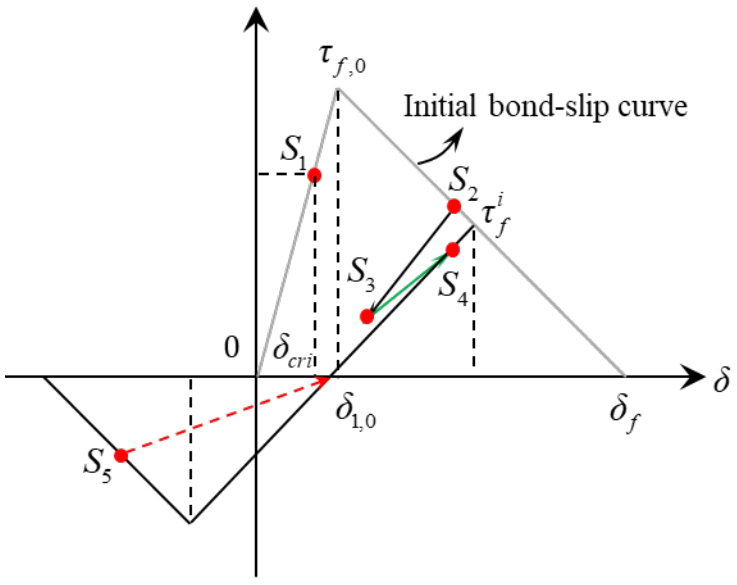


**Fig.3.** Possible states of the nodes under fatigue loading.

For completeness of the model proposed in this paper, a damaged elasticity type of model was assumed when shear stress is reversed. This is highlighted in Fig. 3 by the reversal of the load to point $S_5$. The residual fracture energy during the reverse loading was assumed to remain unchanged. This assumption of the reverse loading model should be updated once better data become available.

## 3 Damage parameter calculation

The fracture work of the FC bonded joints is related to the fracture surface/path. Therefore, when obtaining the bond-slip relationship of the bonded joints, it is important to ensure attention is given to the particular failure mode. Bond-slip behaviour of an interface failing through fracture of a certain surface cannot be used to simulate the behaviour of a bonded joints failing through another fracture surface. As mentioned, the damage-plasticity model used to calculate the initial damage parameter is for the bonded joints failed within concrete. Therefore, in the present study, only the fatigue bond behaviour of FC bonded joints failed within concrete is considered. The other failure modes such as the inter-laminar failure of CFRP plate is dependent on the matrix used in the manufacturing. Data available so far on FC bonded joints under fatigue loading failing in failure modes other than cohesive failure within concrete are inadequate to derive any meaningful conclusions. Therefore, the fatigue bond behaviour of such FC bonded joints failing in failures other than cohesive failure within concrete is considered outside the scope of this study. To calibrate the empirical parameters presented in Eq. (28), only the bond-slip relation of FC bonded joints failed in concrete under fatigue loading should be used.

In the present work, only the bond-slip relation from the tests in Zhou et al. [26] where samples failed in cohesion failure within concrete (i.e., MC50-1, MC50-3, MC50-4, MC60-2 and MC60-3) were used. Specifically, for sample MC50-3, only the data recorded before the failure mode shifted from cohesion failure within concrete to adhesion failure (i.e., before 3000 loading cycles) was used. With the above bond-slip relation under fatigue loading, the unloading/reloading and the transition damage

parameter in recorded cycles were calculated by following the same steps as presented in Zhou et al. [14].

The evolution of the transition stiffness damage parameter at different positions of the bonded joint is presented in Fig.4. The corresponding figures for the unloading/reloading stiffness damage parameter can be found in Zhou et al. [27] and Zhou [37]. Except for the sample MC60-3, the damage accumulation rate in all other samples increased with distance from the loaded end and stabilized after a certain distance (about 60mm away from the loaded end). A slower damage accumulation rate was observed in regions closer to the loaded end due to the existence of compressive stress (the grey hatched zone in Figs. 4(a)-(c)), while damage accumulation rate in regions far away from the loaded end was much larger (in the light red hatched zone in Figs. 4(a)-(c)). As debonding propagates, compressive stress will gradually reduce resulting in gradual increase of damage rate. As debonding propagates away from the loaded end, mode II stresses become dominant resulting in a more stable damage rate. Existing studies show that mode I and mode II stress ratio varies along the bonded joints [34, 38]. While complex stresses including compression and shear stress exists in regions close to the loaded end [34], interfacial stress state becomes mode II dominant as debonding propagates away from the loaded end [39]. The existence of compressive stress could lower down the damage propagation rate compared to that under pure mode II loading. Similar observations were also made in existing experimental studies [10, 40].

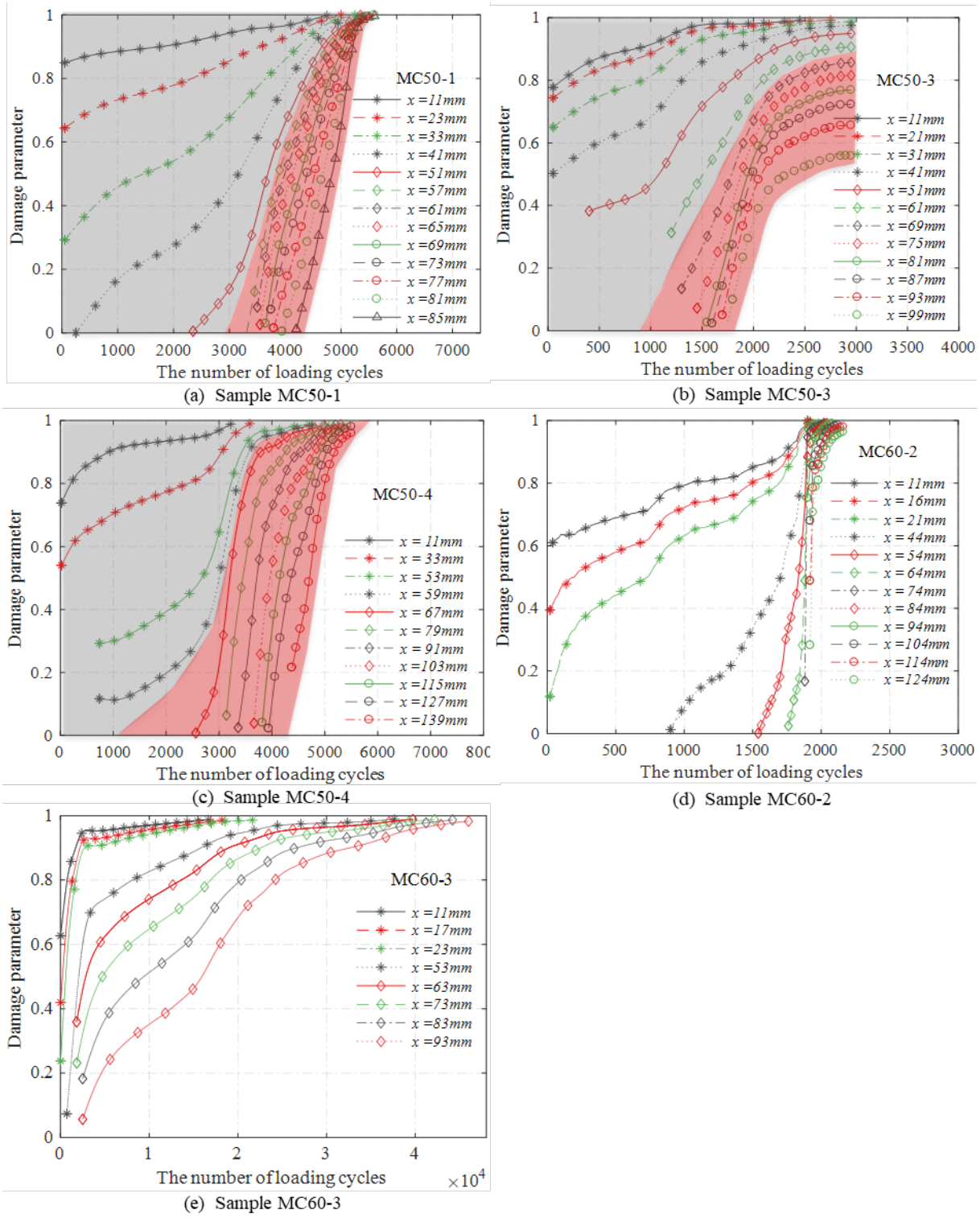


**Fig.4.** The transition stiffness damage parameter evolution at different locations with the number of loading cycles.

For CFRP-to-concrete bonded joints made of 64MPa concrete, it was found that the damage accumulation rate was significantly affected by the maximum fatigue load. A gradually increasing damage rate was observed in the MC60-2 specimen as well as in the MC50-1, -3, and -4 specimens.

However, when debonding propagated approx. 54mm into the bond line away from the loaded end, sudden crack propagations resulted in a steep gradient of the damage parameter accumulation curves as shown in Figs. 4(a)-(d). For the specimen MC60-3 (Fig. 4(e)), the minimum load applied varied during the testing as 11%, 12.5%, 13.9% and 11% of the load-carrying capacity under monotonic loading, which can explain the variation in damage increase rates at different locations [27].

As only the modelling of the interfacial behaviour of FC bonded joints under mode II loading is aimed at in this paper, only the damage propagation curves from the region where damage propagation is dominated by mode II loading (i.e. the middle region of the bond length) were considered in calibrating the empirical parameters in Eq. (28). Considering the sudden cracking observed during the testing of the sample MC60-2 [26], data from that sample was excluded from the calibration. It is obvious from Fig. 4, that data from the middle region of the specimens provide a higher damage accumulation rate than the data from the end regions. Therefore, when using the data from the middle region of the bonded joints, the calibrated parameters will lead to a higher damage accumulation rate prediction than the actual in regions close to the loaded end. As the proposed model will be applied to the whole bonding interface, the fatigue life prediction can be expected shorter than the actual.

## 4 Calibration of the damage accumulation rate model under fatigue loading

The damage parameter evolution curves from different locations of the bonded joints were used to determine the damage accumulation rate for both the unloading/reloading and transition stiffness as a function of the loading parameter ( $\Delta$ ) and the damage parameter ( $D_{ur}$ or $D_{tr}$ ). The slip value ( $\delta_1$ ) corresponding to the peak shear stress under monotonic loading was also obtained through the tests. With the above parameters, a nonlinear regression analysis was carried out using all the test data (Fig. 5). As can be seen in Fig. 5, a higher damage accumulation rate results in lower values of the damage parameter, and the damage accumulation rate tends to decrease as the damage level increases. In addition, for a given damage state, a greater loading parameter will result in a higher damage accumulation rate. In other words, an increase in fatigue damage accumulation rate can be expected

when a greater maximum load and a greater load amplitude are applied. Through a nonlinear regression analysis, expressions for the damage accumulation rate of unloading/reloading and transition stiffness are obtained as:

$$\dot{D}_{ur} = 0.00303 \times \left(1 - D_{ur}\right) e^{\left(-1.678 D_{ur}\right)} \Delta \tag{32}$$

$$\dot{D}_{tr} = 0.00308 \times \left(1 - D_{tr}\right) e^{\left(-1.682 D_{tr}\right)} \Delta \tag{33}$$

The degradation rate of the transition stiffness for a given damage parameter or loading parameter is slightly higher than that of the unloading/reloading stiffness. Significant scatter in data resulted in the relative low fitting score (0.66 and 0.64 represented by the adjusted R-square value). Such variance can be attributed to the dynamic cracking in the FC bonded joints. Typically, during damage propagation, a crack of a certain bonding length can occur at any given time. Inhomogeneity in the concrete microstructure as well as the number of micro cracks at any given stage influence the crack propagation, therefore may lead to different crack propagation rates. However, in developing the theoretical models, concrete is considered as a homogeneous material, thus abrupt variations in crack propagation rate are neglected. Irrespective of the variations observed in test data, a model based on the above-mentioned test data may still provide an averaged damage accumulation rate for the FC bonded joints under mode II dominated loading conditions, which can be considered as a conservative fatigue damage prediction model.

In addition, it is also clear that for FC bonded joints failing in cohesive failure within concrete, the mechanical properties of the concrete play a key role in damage initiation and propagation. The empirical constants in Eqs. (32) and (33) are obtained only from test data covering concrete strengths 50MPa and 64.1MPa. Only two concrete strengths are far from sufficient to derive generally accurate empirical equations. Therefore, much more data covering different concrete strengths are required to develop more accurate functions for Eqns. (32) and (33). Nonetheless, the modelling approach presented in this paper is still generally applicable for all FC bonded joints.

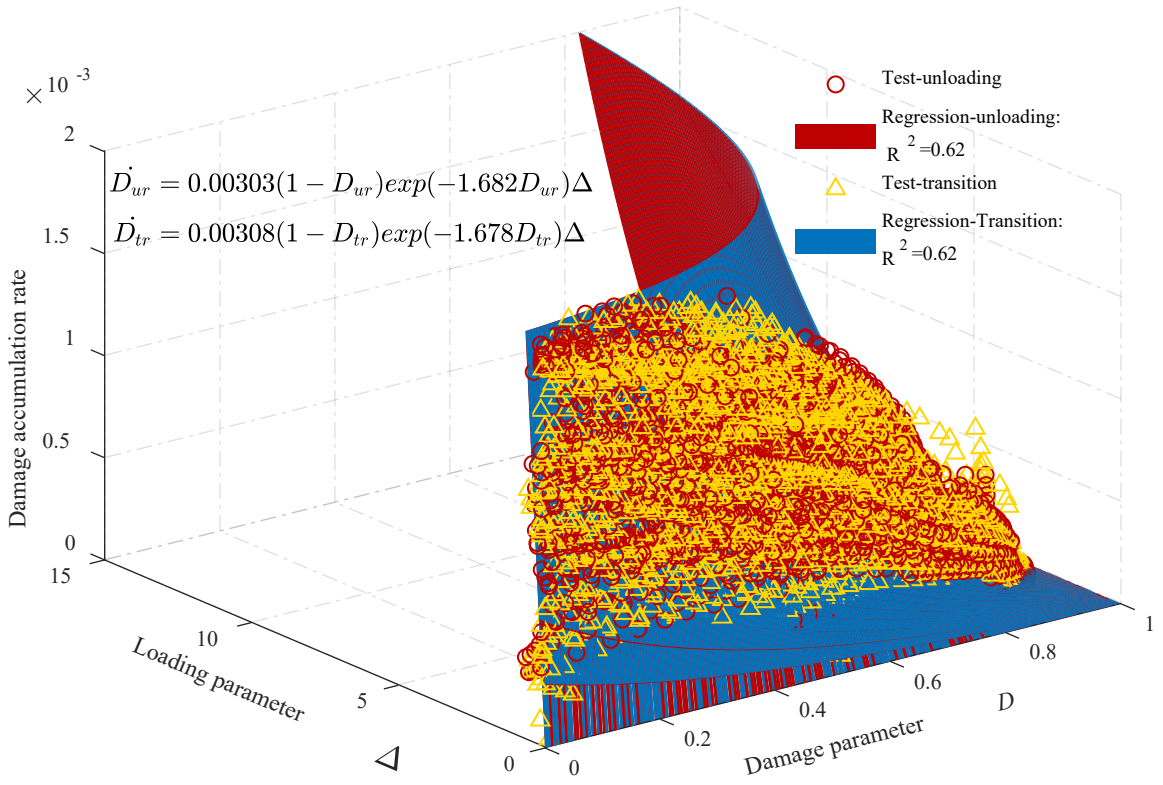


**Fig. 5.** The calibrated model for the damage accumulation rate of CFRP-to-concrete (FC) bonded joints.

## 5 Numerical implementation of the proposed model

To demonstrate the numerical implementation of the proposed mode, the behaviour of a FC single-shear pull-off test specimen under fatigue loading was modelled using the FD method presented in Section 2. Damage evolution due to fatigue loading was calculated using the damage accumulation rate for unloading/reloading and transition stiffness given in Eqs (32) and (33). During the simulation, the state of each node was checked at every loading cycle to determine if the node has reached the range that fatigue damage starts to accumulate (i.e., node slip is greater than the critical ratio $r_{cri}$). Damage accumulation was initiated when reloading occurred. A flow diagram illustrating the calculation algorithm implemented in Matlab [41] to simulate the behaviour of FC bonded joints under mode II fatigue loading is given in Fig. 6.

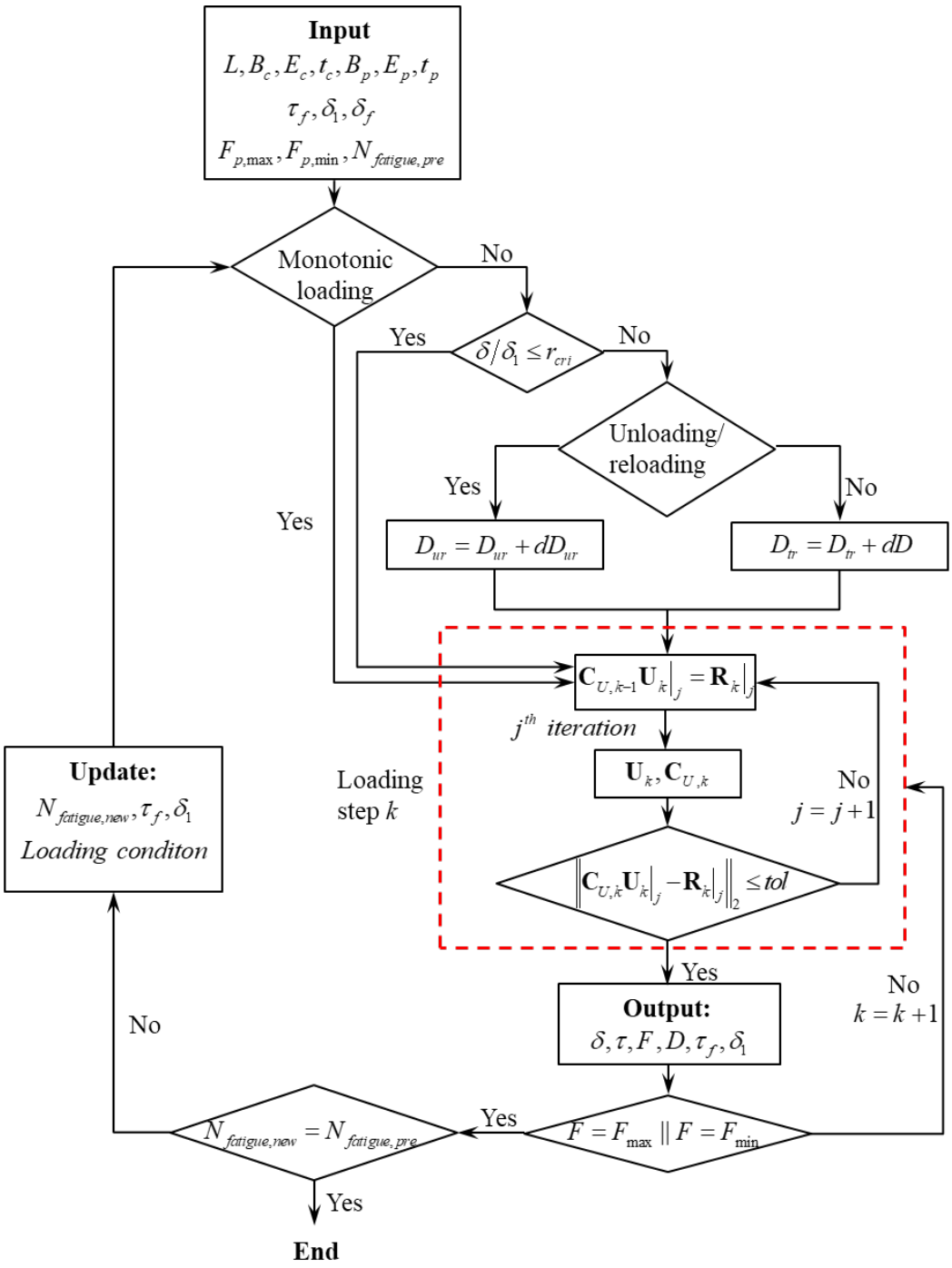


**Fig. 6.** Flow chart of the numerical implementation of the proposed model.

In the algorithm shown in Fig. 6, the material properties ($E_c$, $E_p$), geometry of the bonded joints ($B_p$- width of the FRP plate, $L$- length of the bonded joint, $t_c$-thickness of the concrete block, $t_p$-thickness of the FRP plate), the initial parameters for the bond-slip relation ($\tau_f$- interfacial shear strength, $\delta_1$- slip at interfacial shear strength, $\delta_f$-slip at full damage) under monotonic loading and the fatigue load conditions ($F_{max}$-maximum applied load, $F_{min}$-minimum applied load, $N_{fatigue,pre}$-number of

predefined fatigue loading cycles) are given as input to start the analysis. When the bonded joint is subjected to a monotonic loading condition, the $\delta$ and $\tau$ are calculated through an iterative process for each force increment. The detailed solving process can be found in Ref. [34]. When the fatigue loading is applied to the bonded joints and the maximum interfacial shear stress/slip has reached the threshold value for fatigue damage accumulation (i.e., $\frac{\delta}{\delta_1} \geq r_{crt}$), the $D_{ur}$, and $D_{tr}$ will be calculated and updated for the subsequent calculation. These damage parameters will be further used as input for the iterative solution process. Once a converged solution is obtained (that is when $||\boldsymbol{C}_{U,k}\boldsymbol{U}_k|_j - \boldsymbol{R}_k|_j||_2 \leq tol$, where $tol$ is the tolerance value to accept the convergence), the interfacial slip, stress, damage parameters, and the parameters for the bond-slip relation in the current loading cycle will be used for the subsequent calculation. In each loading cycle, such process will be repeated until the prescribed force is attained. The above process will be looped until the number of loading cycles has reached the predetermined value.

To demonstrate the workability of the proposed model and FD algorithm, behaviour of the specimen MC50-4 from Zhou et al. [27] was simulated using the parameters given in Table. 1. In the numerical simulation, the loading protocol followed in the test was used as the input to control the simulation. The bonded joint was first monotonically loaded to 24kN and then unloaded to 4kN. This was then followed by 2500 cycles of fatigue loading ranging from 4kN to 24kN. Next another 3000 cycles of fatigue loading ranging from 4kN to 25kN were applied. Finally, monotonic loading was applied until full debonding of the bonded joint occurred.

**Table 1.** Parameters used in the simulation of sample MC504

| $E_p$ | $b_p$ | $t_p$ | $E_c$ | $b_c$ | $t_c$ | $\tau_{f,0}$ | $\delta_1$ | $\delta_2$ | $L$ |
|---|---|---|---|---|---|---|---|---|---|
| MPa | mm | mm | MPa | mm | mm | MPa | mm | mm | mm |
| 160000 | 50 | 1.4 | 33446 | 150 | 200 | 7.24 | 0.045 | 0.27 | 300 |

Fig. 7 presents the comparison between the experimental and numerical simulation results in terms of the load-displacement curve at the loaded end. It should be noted that the curves are plotted every 20 cycles as the data was recorded at such frequency in the test. It is obvious that the displacement at the loaded end increased with the loading cycles while the slope of the curve decreased. However, compared to the experimental results, the damage accumulated much faster in the numerical simulation. Unlike the experimental test which failure occurred during the final monotonic loading, the numerical simulation shows that the bonded joint failed when the number of loading cycles was 3500. Such a difference was expected as the proposed model used a faster damage accumulation rate than what was observed in the experiments within the bond length closer to the loaded end. Therefore, predictions tend to provide conservative results. To account for the effects of the compressive/tensile stresses within the bonded joints on the fatigue bond behaviour, the damage accumulation rate must consider the mode mix ratio. Such a model can only be developed once experimental data under mixed mode loading becomes available. However, this is outside the scope of the present study.

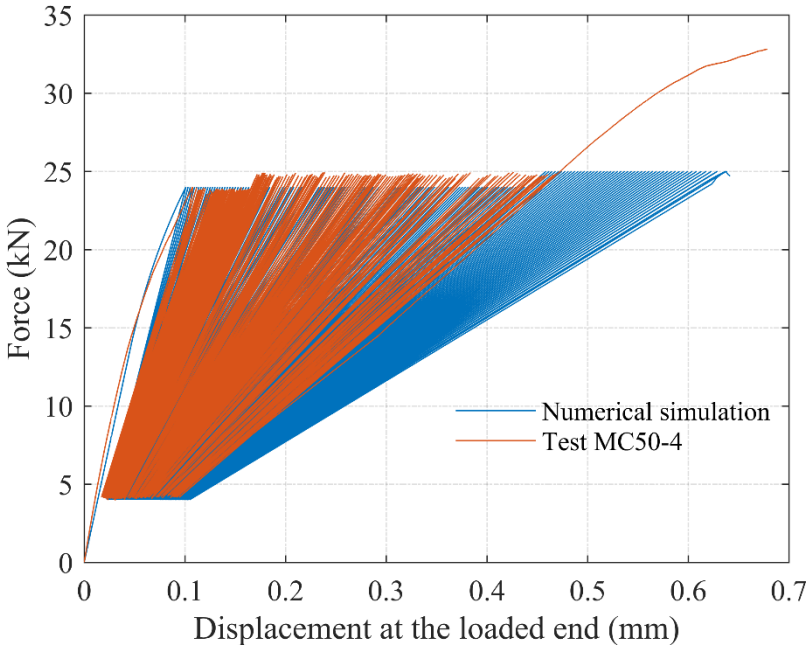


**Fig. 7.** Comparison between numerical simulation and test.

Since the proposed model is aimed at modelling the bond behaviour under mode II loading, only the bond bond-slip curves and damage parameter evolution at 75mm, 85mm, 95mm and 105mm away

475 from the loaded end from both experimental test and numerical simulation are compared in Figs. 8
476 and 9. In the simulation, it is obvious that negative shear stresses occurred in the fatigue loading
477 cycles. Such behaviour is consistent with the experimental findings presented in Zhou et al. [14] for
478 FC bonded joints subjected to cyclic loading. However, interfacial shear stress is always positive in
479 the experimental test results of the fatigue test specimens, as a direct result of the regression analysis
480 method used in obtaining the strain distribution [26]. In obtaining the data from experimental results,
481 noise of data was filtered using a monotonic mathematical expression-based regression analysis
482 method. In doing so, some of the local peaks and valleys (especially if the values are relatively small)
483 in the strain distribution along the bond length were smoothened. Such smoothening is believed to be
484 the reason for not obtaining negative shear stress values, which were clearly present in experimental
485 results of cyclic loading of similar bonded joints [14]. Nonetheless, error caused by the regression
486 analysis is significant only at the later stages of the bond-slip curve when the shear stress reaches zero
487 and the damage parameter is close to 1. Therefore, the overall effect of this error on the global
488 behaviour was considered to be negligible.

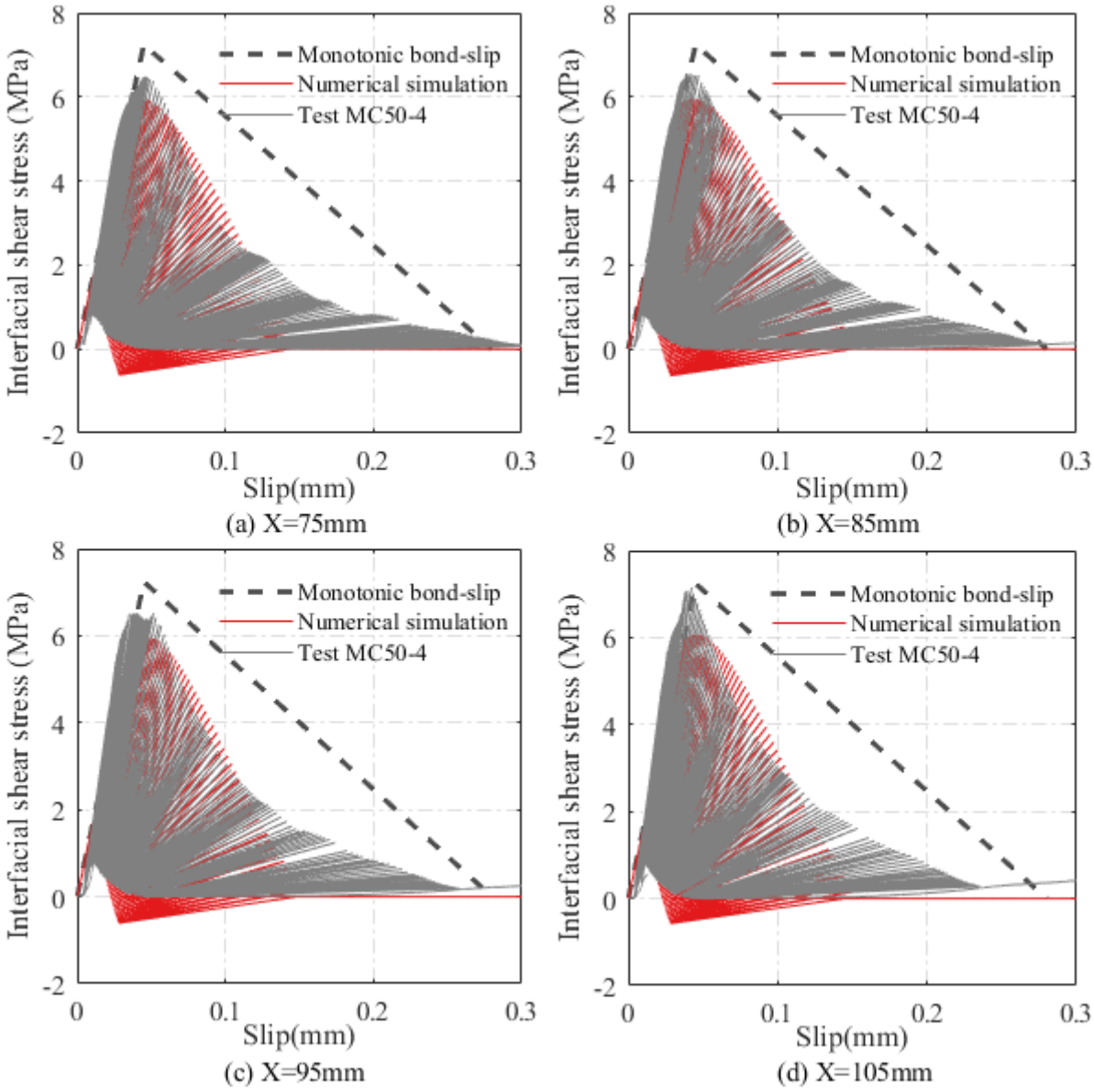


**Fig.8.** Comparison of the bond-slip relation between numerical simulation and test MC30-4 at different locations.

Experimental results of the damage parameter evolution showed a good agreement with the simulation results while the damage parameter is less than 0.8 (Fig. 9). It is assumed that full damage at a node is reached when either the maximum interfacial shear stress value become negative or when a node enters the reversed softening region (Fig. 9). This assumption is employed to ensure the ultimate stress is not negative when the damage parameter reaches 1 during the simulation. As a result of this assumption, a jump in the damage parameter was observed from approximately 0.9 to 1 in the simulation results. For all the experimental data used to calibrate the models proposed in this paper,

499 the maximum loading amplitude was over 65% of the bond strength. Therefore, strict application of
500 the model is also limited to the loading range of the tests, i.e., over 65% of the bond strength. When
501 the maximum load amplitude is over 65% of the bond strength, the damage parameter can expected
502 to be closer to 1 when the maximum shear stress becomes zero. As such, assuming full damage is
503 deemed to be reasonable.

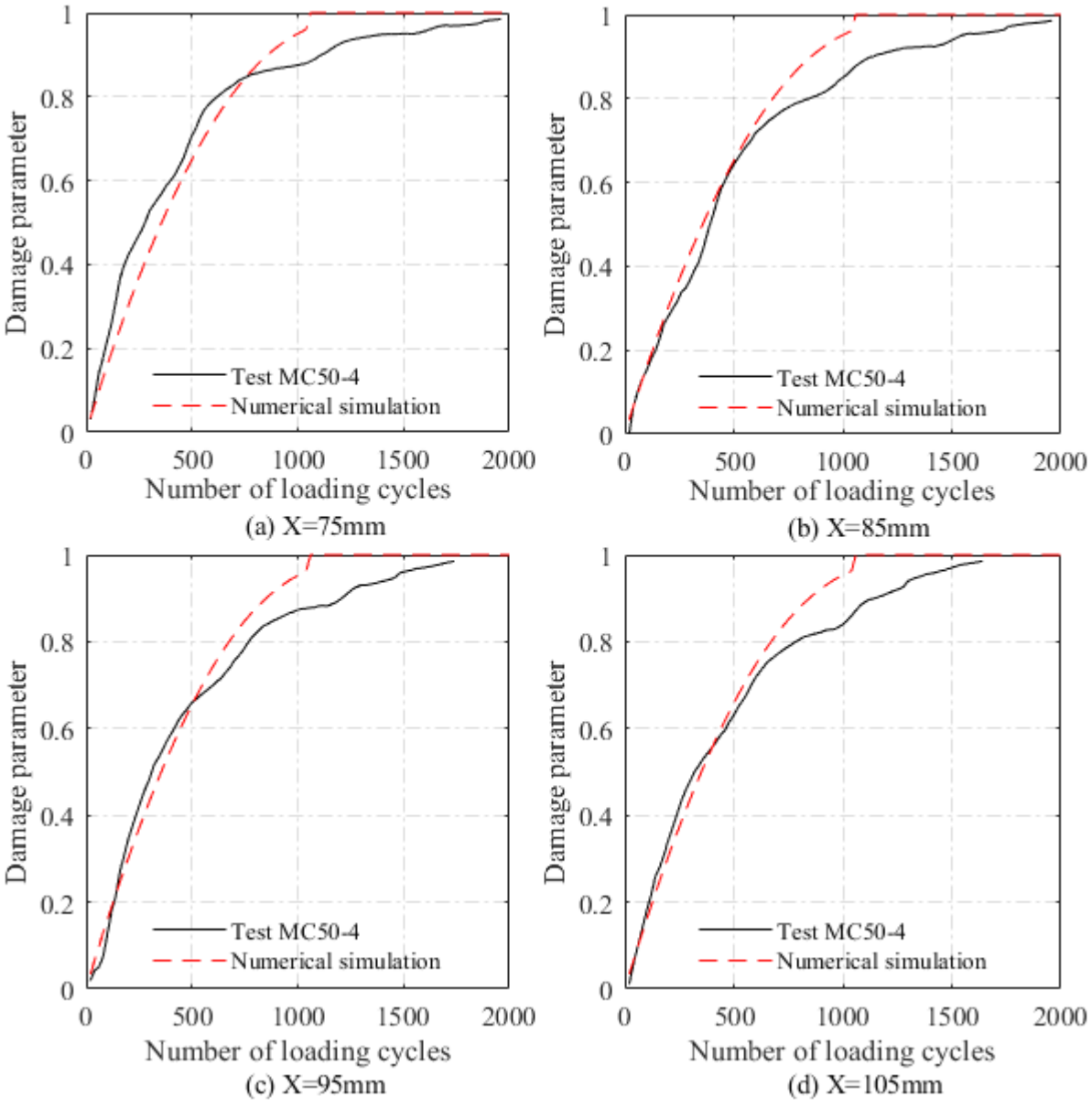


504

505 **Fig. 9.** Comparison of the unloading/reloading damage parameter evolution between numerical
506 simulation and test MC30-4 at different locations.

## 6 Conclusions

In this paper, a numerical model which can predict the bond behaviour of CFRP-to-concrete (FC) bonded joints failing in cohesion failure within concrete under mode II fatigue loading was developed. Based on the comparison between numerical simulations and test results, the following conclusions can be drawn:

1. The fatigue damage accumulation rate was found to vary along the bond length. Fatigue damage accumulation rate closer to the loaded end was much slower than that in regions far away from the loaded end. This low fatigue damage accumulation rate closer to the loaded end is attributed to the existence of compressive stresses in the regions close to the loaded end.
2. It was found that even though the damage level and the applied stress amplitude are the same, the damage accumulation rate at different locations could be different. This is due to brittle, unstable cracking within concrete which are typically not distributed uniformly along the bond length.
3. The damage accumulation rate for the unloading/reloading and transition stiffness were calibrated as a relation between the damage level and the stress amplitude by using the bond-slip relation in regions with mode II dominant loading. Such a model can be used to predict the bond-behaviour of FC bonded joints under mode II fatigue loading.
4. The proposed numerical simulation slightly overestimates the debonding rate and thus provides a conservative prediction for the fatigue life of the bonded joints. This is due to ignoring the beneficial effects from the compressive stresses near the loaded end on reducing the rate of crack propagation, which was done as only mode II loading was considered in the present study. For pure mode II load conditions, the proposed numerical simulation is expected to provide more accurate predictions.
5. A larger test database on the bond behaviour of FC bonded joints under fatigue loading is required to further calibrate and improve the accuracy of the proposed model. In addition,

while the present study is focused on cohesion failure within concrete, numerical models for other interfacial failure modes are worth investigation in future studies.

**Acknowledgement**

The authors are thankful for the financial support received from the Natural Science Foundation of Hunan Province, China (Grant No. 2021JJ40777) to the first author.

**Reference**

[1]. Hollaway, LC and Teng JG. Strengthening and rehabilitation of civil Infrastructures using fibre-reinforced polymer (FRP) composites. 2008: Elsevier Science.

[2]. de Waal, L, Fernando D, Nguyen VT, Cork R, and Foote J. FRP strengthening of 60 year old pre-stressed concrete bridge deck units. Eng. Struct., 2017. 143: p. 346-357.

[3]. Chen, GM, Chen JF, and Teng JG. Behaviour of FRP-to-concrete interfaces between two adjacent cracks: A numerical investigation on the effect of bondline damage. Constr. Build. Mater., 2012. 28(1): p. 584-591.

[4]. Chen, JF and Teng JG. Anchorage strength models for FRP and steel plates attached to concrete. J. Struct. Eng., 2001. 127(7): p. 784-791.

[5]. Lu, XZ, Teng JG, Ye LP, and Jiang JJ. Bond–slip models for FRP sheets/plates bonded to concrete. Eng. Struct., 2005. 27(6): p. 920-937.

[6]. Tao, Y and Chen JF. Concrete damage plasticity model for modeling FRP-to-concrete bond behavior. J. Compos. Constr., 2014. 19(1).

[7]. Yuan, H, Teng JG, Seracino R, Wu ZS, and Yao J. Full-range behavior of FRP-to-concrete bonded joints. Eng. Struct., 2004. 26(5): p. 553-565.

[8]. Yao, J, Teng JG, and Chen JF. Experimental study on FRP-to-concrete bonded joints. Compos. B. Eng., 2005. 36(2): p. 99-113.

[9]. Martinelli, E and Caggiano A. Low-Cycle Fatigue of FRP Strips Glued to a Quasi-Brittle Material. Materials (Basel, Switzerland), 2021. 14(24).

[10]. Mazzotti, C, Savoia M, and Ferracuti B. A new single-shear set-up for stable debonding of FRP–concrete joints. Constr. Build. Mater., 2009. 23(4): p. 1529-1537.

[11]. Ko, H and Sato Y. Bond stress-slip relationship between FRP sheets and concrete under cyclic load. J. Compos. Constr., 2007. 11(4): p. 419-426.

[12]. Martinelli, E and Caggiano A. A unified theoretical model for the monotonic and cyclic response of FRP strips glued to concrete. Polymers, 2014. 6(2): p. 370-381.

563 [13]. Carrara, P and De Lorenzis L. A coupled damage-plasticity model for the cyclic behavior of
564 shear-loaded interfaces. J. Mech. Phys. Solids, 2015. 85(1): p. 33-53.
565 [14]. Zhou, H, Fernando D, Chen GM, and Kitipornchai S. The quasi-static cyclic behaviour of
566 CFRP-to-concrete bonded joints: An experimental study and a damage plasticity model. Eng.
567 Struct., 2017. 153: p. 43-56.
568 [15]. Mazzotti, C and Savoia M. FRP-concrete bond behaviour under cyclic debonding force. Adv.
569 Struct. Eng, 2009. 12(6): p. 771-780.
570 [16]. Gao, WY, Teng JG, and Dai JG. Effect of temperature variation on the full-range behavior of
571 FRP-to-concrete bonded joints. J. Compos. Constr., 2012. 16(6): p. 671-683.
572 [17]. Bizindavyi, L, Neale KW, and Erki MA. Experimental investigation of bonded fiber
573 reinforced polymer-concrete joints under cyclic loading. J. Compos. Constr., 2003. 7(2): p.
574 127-134.
575 [18]. Diab, HM, Wu ZS, and Iwashita K. Theoretical solution for fatigue debonding growth and
576 fatigue life prediction of FRP-concrete interfaces. Adv. Struct. Eng, 2009. 12(6): p. 781-792.
577 [19]. Carloni, C, Subramaniam KV, Savoia M, and Mazzotti C. Experimental determination of
578 FRP–concrete cohesive interface properties under fatigue loading. Compos. Struct., 2012.
579 94(4): p. 1288-1296.
580 [20]. Zhang, W. Experimental study on fatigue behaviour of CFRP plates externally bonded to
581 concrete substrate. Struct. Concr., 2016. 17(2): p. 235-244.
582 [21]. Zhang, W. Prediction of the bond–slip law between externally bonded concrete substrates and
583 CFRP plates under fatigue loading. Int. J. Civ. Eng., 2017.
584 [22]. Li, K, Cao SY, and Wang XL. Experimental study on the fatigue endurance of the CFRP-
585 concrete interface. J. Compos. Constr., 2014. 19(4): p. 04014075.
586 [23]. Li, K, Cao S, Yang Y, and Zhu J. Bond-slip relationship for CFRP sheets externally bonded
587 to concrete under cyclic loading. Materials (Basel, Switzerland), 2018. 11(3).
588 [24]. Yun, YC, Wu YF, and Tang WC. Performance of FRP bonding systems under fatigue loading.
589 Eng. Struct., 2008. 30(11): p. 3129-3140.
590 [25]. Ferrier, E, Bigaud D, Hamelin P, Bizindavyi L, and Neale K. Fatigue of CFRPs externally
591 bonded to concrete. Mater. Struct., 2005. 38(1): p. 39-46.
592 [26]. Zhu, JT, Wang XL, Kang XD, and Li K. Analysis of interfacial bonding characteristics of
593 CFRP-concrete under fatigue loading. Constr. Build. Mater., 2016. 126: p. 823-833.
594 [27]. Zhou, H, Fernando D, Thuan Nguyen V, and Dai J-G. The bond behaviour of CFRP-to-
595 concrete bonded joints under fatigue cyclic loading: An experimental study. Constr. Build.
596 Mater., 2021. 273: p. 121674.

[28]. Carloni, C and Subramaniam KV. Investigation of sub-critical fatigue crack growth in FRP/concrete cohesive interface using digital image analysis. Compos. B. Eng., 2013. 51: p. 35-43.
[29]. Yuan, H, Luo G, Liu C, and Zeng L. Interfacial properties of CFRP sheets and concrete subjected to variable amplitude fatigue loading. Struct. Concr., 2021.
[30]. Al-Saoudi, A, Al-Mahaidi R, Kalfat R, and Cervenka J. Finite element investigation of the fatigue performance of FRP laminates bonded to concrete. Compos. Struct., 2019. 208: p. 322-337.
[31]. Chalot, A, Michel L, and Ferrier E. Experimental study of external bonded CFRP-concrete interface under low cycle fatigue loading. Compos. B. Eng., 2019. 177.
[32]. Wei, MW, Xie JH, Huang PY, and Huang KH. Fatigue behaviour of the bond interface between carbon fibre‐reinforced polymer sheets and concrete. Fatigue Fract. Eng. Mater. Struct., 2020. 43(9): p. 2116-2129.
[33]. Zhang, W, Tang Z, Yang Y, Wei J, and Stanislav P. Mixed-mode debonding behavior between CFRP plates and concrete under fatigue loading. J. Struct. Eng.-ASCE, 2021. 147(5): p. 04021055.
[34]. Carrara, P and Ferretti D. A finite-difference model with mixed interface laws for shear tests of FRP plates bonded to concrete. Compos. B. Eng., 2013. 54: p. 329-342.
[35]. Roe, KL and Siegmund T. An irreversible cohesive zone model for interface fatigue crack growth simulation. Eng. Fract. Mech., 2003. 70(2): p. 209–232.
[36]. Lu, XZ, Ye LP, Teng JG, and Jiang JJ. Meso-scale finite element model for FRP sheets/plates bonded to concrete. Eng. Struct., 2005. 27(4): p. 564-575.
[37]. Zhou, H. Behaviour of FRP-to-concrete bonded joints under cyclic and thermal loading, in School of Civil Engineering. 2019, The University of Queensland: Brisbane, Australia.
[38]. Lin, JP and Wu YF. Numerical analysis of interfacial bond behavior of externally bonded FRP-to-concrete joints. J. Compos. Constr., 2016. 20(5): p. 04016028.
[39]. Fernando, D. Bond behaviour and debonding failures in CFRP-strengthened steel members, in Department of Civil and Structural Engineering. 2010, The Hong Kong Polytechnic University: HongKong, China.
[40]. Zhou, YW, Wu YF, and Yun YC. Analytical modeling of the bond–slip relationship at FRP-concrete interfaces for adhesively-bonded joints. Compos. B. Eng., 2010. 41(6): p. 423-433.
[41]. The Mathworks Inc. MATLAB version 9.3.0.713579 (R2017b). 2017: Natick, Massachusetts.